Atmos. Chem. Phys. Discuss., 14, 23375–23413, 2014
www.atmos-chem-phys-discuss.net/14/23375/2014/
doi:10.5194/acpd-14-23375-2014

Atmospheric Chemistry and Physics Discussions

Aerosol physicochemical properties and implication for visibility during an intense haze episode during winter in Beijing

Y. H. Wang[1,2], **Z. R. Liu**[1], **J. K. Zhang**[1], **B. Hu**[1], **D. S. Ji**[1], **Y. C. Yu**[1], **and Y. S. Wang**[1,2]

[1]State Key Laboratory of Atmospheric Boundary Layer Physics and Atmospheric Chemistry (LAPC), Institute of Atmospheric Physics, Chinese Academy of Science, Beijing 100029, China
[2]College of Atmospheric Science, Lanzhou University, Lanzhou, 730000, China

Received: 1 June 2014 – Accepted: 27 August 2014 – Published: 10 September 2014

Correspondence to: Y. S. Wang (wys@mail.iap.ac.cn)

Published by Copernicus Publications on behalf of the European Geosciences Union.

Abstract

The evolution of physical, chemical and optical properties of urban aerosol particles was characterized during an extreme haze episode in Beijing, PRC from 24 January through 31 January 2013 based on in-situ measurements. The average mass concentrations of PM_1, $PM_{2.5}$ and PM_{10} were $99 \pm 67\,\mu g\,m^{-3}$ (average ± stdev), $188 \pm 128\,\mu g\,m^{-3}$ and $265 \pm 157\,\mu g\,m^{-3}$, respectively. A significant increase in $PM_{1-2.5}$ fraction was observed during the most heavily polluted periods. The average scattering coefficient ($\lambda = 550\,nm$) was $877 \pm 624\,M\,m^{-1}$. An increasing relative amount of coarse particles can be deduced from the variations of backscattering ratios, asymmetry parameter and scattering Ångström exponent. Particle number size distributions between 14 nm and 2500 nm diameter showed high number concentrations, particularly in the nucleation mode and accumulation modes. Size-resolved chemical composition of submicron aerosol from a High Resolution-ToF-Aerosol Mass Spectrometer showed that the mass concentration of organic, sulfate, nitrate, ammonium and chlorine mainly resided on 500 nm to 800 nm (vacuum diameter) particles, and sulfate and ammonium contributed most to particle growth during the most heavily polluted day (28 January).

Increasing relative humidity and stable synoptic conditions on 28 January combined with heavy pollution, lead to enhanced water uptake by the hygroscopic submicron particles and formation of secondary aerosol, maybe the main reasons for the severity of the haze episode. Light scattering apportionment showed that organic, ammonium sulfate, ammonium nitrate and ammonium chloride compounds contributed to light scattering fractions of 57 %, 23 %, 10 % and 10 %, respectively. This study indicated that the organic component in submicron aerosol plays an important role in visibility degradation in this haze episode in and around Beijing.

ACPD
14, 23375–23413, 2014

1 Introduction

Atmospheric aerosol particles play significant role in radiation balance and climate forcing through direct scattering and absorption of solar radiation (Anderson et al., 2003; Poschl, 2005; Ramanathan et al., 2001); they can act as cloud condensation nuclei (CCN) and thereby change the cloud albedo and lifetime (Twomey, 1977). Accordingly, the radiative properties of clouds are influenced by aerosol indirectly (Kaufman et al., 2005; Koren et al., 2005; Lohmann and Feichter, 2005). Furthermore, the general public has to pay special attention to atmospheric aerosol due to its deleterious effects on human health and degradation of visibility (Nel, 2005; Watson, 2002), which are closely related to the chemical components, morphology, mixing state, size distribution and hygroscopic properties of aerosol particles.

Along with the rapid economic growth in China, its capital city Beijing has suffered substantially from air quality deterioration and visibility degradation, though the total aerosol mass concentration has decreased in Beijing in the last ten years. Accompanied by frequent fog-haze days, the visibility in Beijing has decreased dramatically to an unacceptable level. The visibility frequency between 2 km and 10 km has increased from 37 % in 1999 and 43 % in 2007 (Zhang et al., 2010). The mass loading of fine aerosol particles and their precursors, e.g. NH_3, volatile organic compounds (VOCs), SO_2 and NO_x, can accumulate to high levels within the planetary boundary layer, especially during persistent synoptic stagnation and strong temperature inversions (Zhang et al., 2013). In the past decade, much research has been done to characterize the chemical and physical properties of aerosol particles in Beijing and its surrounding regions. These studies mainly focus on the following aspects:

1. Chemical composition, evaluation and sources apportionment based on filter sampling and Aerosol Mass Spectrometry (AMS) (Huang et al., 2010b; Sun et al., 2006; Zhang et al., 2014).

2. Mass concentration and optical properties of aerosol particles using in-situ measurements or combined with MODIS satellite remote sensing optical depth prod-

ACPD
14, 23375–23413, 2014

ucts (He et al., 2009; Huang et al., 2010a; Li et al., 2010; Qu et al., 2010; Wang et al., 2012a; Yang et al., 2009).

3. Aerosol hygroscopic properties, number size distributions, mixing state and implications for CCN activity, visibility, new particle formation, air pollution and radiative forcing (Chen et al., 2012; Cheng et al., 2012; Deng et al., 2013; Liu et al., 2013; Ma et al., 2012; Meier et al., 2009; Pan et al., 2009; Quan et al., 2011; Wehner et al., 2008; Wu et al., 2007; Zhang et al., 2011, 2010).

The above mentioned studies, based on either long or short observations provide us with comprehensive knowledge of aerosol properties on days with near average aerosol concentration levels. However, only a few studies were carried out on more highly polluted days, and these studies mainly focus on variations of chemical composition with the evaluation of synoptic conditions and planetary boundary layer dynamics. (Huang et al., 2010a; Wang et al., 2012b; Zhao et al., 2013). The interaction between chemical and physical aerosol properties was seldom investigated during haze episodes. Therefore, comprehensive studies of physical, optical and chemical properties using high resolution measurements are necessary for a better knowledge of aerosol evolution processes and related visibility degradation during pollution episodes in Beijing.

An intense pollution episode occurred in central and eastern China from 24 through 31 January 2013. The hourly averaged PM_{10} exceeded 600 $\mu g\,m^{-3}$ and non-refractory submicron particle (NR-PM_1) exceeded 400 $\mu g\,m^{-3}$ (Wang et al., 2014a), which is the most extreme haze episode in Beijing in the last decades as far as we know. Here, we use data of high resolution AMS, precursor gases, particle number size concentration and mass concentration combined with aerosol light scattering properties to investigate details of aerosol processing, evolution over time and chemical apportionment of light scattering during this haze episode.

ACPD
14, 23375–23413, 2014

2 Methodology

2.1 Site information and instruments introduction

The observation site where aerosol sampling was carried out was on the roof (~ 15 m high) of a laboratory building in the yard of the Institute of Atmospheric Physics (IAP), Chinese Academy of Science, which is located between the 3rd and 4th ring roads of northeast Beijing (Zhang et al., 2014).

An integrating nephelometer (Model 3563, TSI inc., Minnesota, USA) was used to measure the total light scattering and hemispheric back scattering coefficients (for angles between 7–170°, respectively) of low RH aerosol at wavelengths of 450, 550 and 700 nm, no size-selective inlets were used. The nephelometer was operated at 5 L min^{-1} with data resolution of one minute. The calibration was conducted every month with filtered air and CO_2 as prescribed by the manufacturer. Subsequently, the data were corrected for truncation errors and the non-lambertian light source based on the measured Ångström exponents (Anderson and Ogren, 1998). On average, the corrected values were within 10 % of the measured values. The mass concentration of PM_{10} (particulate matter with aerodynamic diameter less than 10 µm) and $PM_{2.5}$ (particulate matter with aerodynamic diameter less than 2.5 µm) were measured by a Thermo TEOM 1400AB/8500 FDMS (Filter Dynamic Measurement System). The mass concentration of PM_1 was determined using a Thermo TEOM 1400.

The particle number-size distribution between 14–2500 nm diameter was measured by a Scanning Mobility Particle Sizer (SMPS, TSI inc., Minnesota, USA), comprising a model TSI 3080 electrostatic classifier and a model TSI 3775 condensation particle counter (CPC), and an Aerodynamic Particle Sizer (APS, Model 3321, TSI inc., Minnesota, USA). The SMPS data covered the particle size range from 14–533 nm, and the APS covered from 542 to 2500 nm. The size-dependent diffusional and gravitational losses for the inlet line have been corrected by using the empirical functions given by Willeke and Baron (1993). The data collected from these two instruments was merged

ACPD
14, 23375–23413, 2014

into one particle size spectrum matrix (14 nm to 2500 nm) according to the method of Liu et al. (2014) and Beddows et al. (2010).

The aerosol chemical composition was acquired using an Aerodyne High-Resolution Time-of-Flight Aerosol Mass Spectrometer (HR-ToF-AMS, or AMS, Aerodyne Research Inc., Billerica, MA, USA). The organic matter, sulfate, nitrate, ammonium and chlorine in non-refractory submicron particle mass-size distribution (NR-PM_1) were determined under V and W ion optical modes alternatively every 7.5 min. Detailed information of data analysis, collection efficiency (CE) and relative ionization efficiency of the instrument were introduced by Zhang et al. (2014). Simultaneously, the gaseous pollutants (NO, NO_x, CO, O_3 and SO_2) were measured using Thermo instruments (series of 42i, 48i, 49i and 43i, respectively, Thermo Fisher Scientific, Franklin, Massachusetts, USA). Detailed introduction and calibrations were given by (Tang et al., 2012; Wang et al., 2014b).

An automatic meteorological observation instrument (Milos520, Vaisala, Finland) was used at the site to obtain meteorological parameters (relative humidity, air temperature, wind speed and direction). The time base for all data in the study is Beijing zone time (UTC + 8).

3 Results and discussion

3.1 Aerosol mass concentration and meteorological parameters

Figure 1 shows the mass concentrations of PM_1, $PM_{1-2.5}$, $PM_{2.5-10}$ and mass concentration ratios of $PM_1/PM_{2.5}$, $PM_{2.5}/PM_{10}$ during the period. The averaged mass concentration of PM_1, $PM_{2.5}$ and PM_{10} are $99.1 \pm 67.1\ \mu g\ m^{-3}$, $188.3 \pm 128.8\ \mu g\ m^{-3}$ and $265.2 \pm 157.1\ \mu g\ m^{-3}$, indicative of the high level of aerosol pollution associated with this episode. The averaged mass ratios of $PM_1/PM_{2.5}$ and $PM_{2.5}/PM_{10}$ are 0.56 ± 0.16 and 0.64 ± 0.15. As we can see in Fig. 1b, the mass ratio of $PM_1/PM_{2.5}$ is higher, while the ratio of $PM_{2.5}/PM_{10}$ is lower before 28 January, indicating that PM_1 dominated

ACPD
14, 23375–23413, 2014

the total mass. Figure S1 in the Supplement displays meteorological parameters during the episode. During this period, the average wind speed was 2.5 m s^{-1}. Figure S2 in the Supplement show an overview of wind rose for the local wind, the wind was mainly in the southerly and northerly quadrant, which can bring relative dirty or clean air masses, respectively. Figure 2 exhibits 72 h backward trajectories of air parcel every 3 h using Hysplit model from a height of 100 m, with a total of six clusters yielded (http://ready.arl.noaa.gov/HYSPLIT.php). We should clarify that the southern area of Beijing often suffers a more polluted atmosphere than northern area due to more of cities and much of population. The clusters of 1 to 5 are from northern directions, with clean air and high transport height. Also, long transport way within 72 h implies that those air parcels have a high transport speed compared with cluster 6. The cluster 6, from southern and local direction with a fraction of 47 %, has the most frequency. The cluster has a low transport height and speed, resulting in a sufficient loading of surface air pollutions compared with other clusters. We also present sounding data in Beijing from university of Wyoming twice a day (http://weather.uwyo.edu/upperair/), as shown in Fig. 3. These lines with different color represent sounding curves during the observation period. It is worth noting that an inversion layer at 1000 m to 1500 m exists after 27 January. Particularly at 08:00 of 28 January (Beijing time), the lapse ratio of temperature is nearly −0.6°/100 m, which means a very stable synoptic condition.

The aerosol concentration increased gradually and reached the maximum values at 12:00 of 29 January, with PM_1, $PM_{2.5}$ and PM_{10} values of 243.1 μg m^{-3}, 504.6 μg m^{-3} and 620.8 μg m^{-3}. The detailed interpretations of the high values will be presented in following section. Thereafter, the aerosol concentrations decreased rapidly to a lower level. The mass ratios of $PM_1/PM_{2.5}$ and $PM_{2.5}/PM_{10}$ showed opposite pattern of time variation during the period, indicating a decreasing fraction of PM_1 compared to $PM_{2.5}$ and an increasing fraction of $PM_{2.5}$ compared to PM_{10} with increasing aerosol pollution. It is worth noting that the increase of $PM_{1-2.5}$, as showed in Fig. 1a, was greatest during the period 28 to 29 January.

ACPD
14, 23375–23413, 2014

3.2 Aerosol optical properties at three wavelengths

The aerosol scattering coefficient (σ_{sp}) and backscattering coefficient (σ_{bsp}) can be directly measured by the nephelometer and then aerosol backscattering fraction (b_λ), scattering Ångström exponent ($Å_{sp}$) and asymmetry parameter (g_λ) can be calculated. However, the latter three optical parameters have rarely been reported in Beijing using surface measurements. The aerosol light scattering coefficients show the same pattern as mass concentration of PM, as shown in Fig. 4. Table 1 shows the statistics of the aerosol optical properties during this haze episode, the average aerosol scattering coefficients σ_{sp}^{450},σ_{sp}^{550} and σ_{sp}^{700} are $1088.5 \pm 748.1\,M\,m^{-1}$, $877.2 \pm 624.2\,M\,m^{-1}$ and $718.4 \pm 530.8\,M\,m^{-1}$, respectively. After converting the 550 nm aerosol light scattering coefficients to 525 nm,the average σ_{sp} at 525 nm during this haze episode was 3.2 times greater than the yearly averaged values at 525 nm reported by He et al. (2009) at another urban site in Beijing. The average aerosol backscattering coefficients σ_{bsp}^{450}, σ_{bsp}^{550} and σ_{bsp}^{700} are $134.4 \pm 87.1\,M\,m^{-1}$, $108.1 \pm 71.1\,M\,m^{-1}$ and $98.7 \pm 66.5\,M\,m^{-1}$, as presented in Fig. 4b. During the whole campaign, σ_{sp} and σ_{bsp} at three wavelengths were highly correlated. Both σ_{sp} and σ_{bsp} increased gradually from 24 to 29 January and decreased sharply to lower levels, consistent with the variations of aerosol mass concentration.

The backscattering ratio, which is also called the hemispheric backscatter fraction, is the ratio of light scattered in the backward hemisphere to the total light scattered by particles. The backscattering ratio is related to particle size distribution. It can be calculated as following;

$$b_\lambda = \frac{\sigma_{bsp}^{\lambda}}{\sigma_{sp}^{\lambda}} \quad (1)$$

The average b_λ at three wavelengths are 0.13 ± 0.02, 0.14 ± 0.02 and 0.15 ± 0.02, respectively. A higher value of b_λ at 700 nm indicates relatively more small sized particles

ACPD
14, 23375–23413, 2014

that scatter light in the backward hemisphere. The scattering Ångström exponent ($Å_{sp}$) represents the wavelength dependence of scattering coefficient and can be related to the slope of the number-size distribution or the mean size and relative concentrations of the accumulation and coarse mode aerosol. It is calculated using any two of three channels as follows;

$$Å = -\frac{\log\left(\sigma_{sp}^{\lambda_1}\right) - \log\left(\sigma_{sp}^{\lambda_2}\right)}{\log(\lambda_1) - \log(\lambda_2)} \quad (2)$$

The average $Å_{450/550}$ and $Å_{550/700}$ are 1.2 ± 0.3 and 0.94 ± 0.3. The average $Å_{450/700}$ is 1.1 ± 0.3, which is smaller than the values of 1.46 in Guangzhou (Garland et al., 2008) and 1.7 reported by (Titos et al., 2012) in Spain, which indicated a more dominant coarse particle mode compared with the other locations.

The asymmetry parameter g is a fundamental parameter for radiative transfer calculation, and is defined as the intensity-weighted averaged cosine of the scattering angle:

$$g_\lambda = \frac{1}{2}\int_0^\pi \cos\theta P(\theta)\sin\theta \mathrm{d}\theta \quad (3)$$

Where θ is the angle between incident light and scattering direction and $P(\theta)$ is the angular distribution of scattered light (the phase function). The value of g_λ ranges between -1 for entirely backscattered light to $+1$ for entirely forward scattered light. A fit equation based on plot relating b_λ and g applied by Andrews et al. (2006) was used as in Eq. (4), because no measurements can obtained g values of atmospheric aerosol directly yet.

$$g_\lambda = -7.143889 \cdot b_\lambda^3 + 7.464439 \cdot b_\lambda^2 - 3.9356 \cdot b_\lambda + 0.9893 \quad (4)$$

The average value of g_λ at 450 nm, 550 nm and 700 nm are 0.58 ± 0.04, 0.59 ± 0.05 and 0.54 ± 0.05. The three parameters of b_λ, $Å_{sp}$ and g_λ can show a relative contribution of

ACPD
14, 23375–23413, 2014

particle size to light scattering. During 24 and 25 January, b_λ and $Å_{sp}$ showed higher values, while g_λ showed lower ones, as showed in Fig. 4. However, the opposite situation occurred when the haze developed. Especially during 28, 29 and 30 January, the days of the highest pollution levels, lower values of g_λ and higher values of b_λ and $Å_{sp}$ occurred, which indicates an increasing fraction of relative coarse aerosol, consistent with the variation pattern of $PM_1/PM_{2.5}$ showed in Fig. 1b.

3.3 Particle number size distribution

The particle number-size distribution during 25 to 31 January is shown in Fig. 5. The particle number concentration peaked at a diameter around 100 nm. These particles are mainly from direct emissions from vehicles, cooking and new particle formation (Shi et al., 2001). The nucleation mode (14–25 nm), Aitken mode (25–100 nm), accumulation mode (100–1000 nm) and coarse mode (1000–2500 nm) concentrations with time are presented in Fig. 6. The nucleation mode particles showed the highest number concentration during the period, with an average value greater than 1.5×10^6 cm^{-3}, indicating large emission of reactive or low volatility, aerosol precursor gases (e.g. sulfur dioxide and organic vapors). The least particle number concentration was in coarse mode ($D_m > 1000$ nm), with an average value of 3.18×10^3 cm^{-3}. The Aitken mode and accumulation mode also showed high number concentrations, with the average values of 1.90×10^5 cm^{-3} and 1.01×10^6 cm^{-3}. Compared to three years of measurements of particle number concentration at another urban site in Beijing, the number concentrations of nucleation, Aitken and accumulation mode concentrations during this haze episode are more than 170 times, 10 times and 120 times greater, respectively (Hu et al., 2009). The nucleation mode and Aitken mode particle showed a significant increase at mid-day on 28 January, while the accumulation mode particle did not. This may be due to our research site location in a typical urban area with roads and restaurants around it; emissions from vehicle and cooking also contributed at this time. It is worth noting that coarse mode particle concentration was highest on the 28 and 29 January, which is consistent with the pattern of $PM_{2.5}/PM_{10}$. After the coagulation process,

ACPD
14, 23375–23413, 2014

the number concentrations of nucleation mode and Aitken mode particle decreased on 12:00 LT of 30 January, as is shown in Fig. 6.

3.4 Aerosol chemical properties

Chemical compositions, mass fractions, O : C ratio and m/z 44 of NR-PM_1 are presented in Fig. 7a–c. The average mass concentrations of organic, sulfate, nitrate, ammonium and chloride are $62.1 \pm 46.1\,\mu g\,m^{-3}$, $28.4 \pm 22.1\,\mu g\,m^{-3}$, $37.2 \pm 30.6\,\mu g\,m^{-3}$, $17.4 \pm 12.7\,\mu g\,m^{-3}$ and $5.5 \pm 4.2\,\mu g\,m^{-3}$. The organic component was the dominant one in NR- PM_1, with an average mass fraction of $44.9\% \pm 11.7\%$. Sulfate and nitrate species concentrations were also high, particularly during haze episodes as in 28 and 29 January.

AMS enables the real time determination of size-resolved chemical composition of different particle mode as a function of time. Figure 8 shows the temporal variations of the organic (a), sulfate (b), nitrate (c), ammonium (d) and chloride (e) size distributions. The organic and chloride containing particles displayed a slightly broader distribution than the other three species. The five aerosol components mainly reside in the accumulation mode with vacuum aerodynamic diameters around 700 nm. Note that the AMS size distributions here are shown as a function of vacuum aerodynamic diameter, D_{va}, which is the aerodynamic diameter measured under free-molecular regime flow conditions. Based on the research by (Zhang et al., 2004) in Pittsburgh PA, USA, an average aerosol bulk density 1.5 was assumed in this study. To a first approximation, 700 nm in D_{va} corresponds roughly to 470 nm in physical diameter for spherical particles. It is worth noting that particles with optical diameters between 100 nm and 1000 nm have the highest scattering efficiency in the visible range (Liou, 2002), so a high concentration at this optimum aerosol size will lead to high light scattering and worse visibility during the period.

These five aerosol components all showed high concentrations from the afternoon of 28 January to noon on the 29 January, corresponding with the highest mass loading and light scattering of the overall pollution period. The detailed behaviors of particle

ACPD
14, 23375–23413, 2014

number concentration, size-resolved organic, sulfate, nitrate and ammonium on 28 January are presented in Fig. S4 in the Supplement. The particle number concentration showed a burst at nearly 12:00 LT, with D_m less than 100 nm. Observations by Sakurai et al. (2005) in Atlanta, GA, USA recognized this as a plume related to a new particle formation event. The event was accompanied by advection of local emissions. However, an increasing concentration of aerosol chemical components at about 11:00 LT on 28 January was observed by AMS as shown in Fig. S4 in the Supplement. The mass concentrations mainly reside on between 300 nm and 1000 nm in vacuum diameter. This may be due to the accumulation of air pollutants in the metropolitan region due to boundary layer stagnation. As we can see in Fig. S1 in the Supplement, the meteorological parameters were characterized by calm wind, low RH and increasing temperature in the morning, which leads to a stable boundary layer. Then, with increasing surface temperature and PBL height, the dilution causes the aerosol concentration to decrease in the afternoon. The concentrations of sulfate, ammonium and nitrate showed an increasing trend from 18:00 LT. (1) Increasing RH may enhance the heterogeneous reaction of SO_2 and NH_3 to produce sulfate and nitrate. (2) Decreased PBL height at night leads to accumulation of air pollutant. (3) High level of NO_x promotes the conversion of SO_2 to sulfate according to a recent study (He et al., 2014). All of the above aspects results in the mass concentration of sulfate and ammonium had a distinct particle growth event with diameter between 100 nm and 500 nm on 28 January.

3.5 Increased formation of Secondary Organic Aerosol (SOA) during haze pollution episode

Figure 10 shows the variation of signal of m/z 44 as a function of organic aerosol mass concentration and the influence of relative humidity. The frequency distributions of organic mass and m/z 44 during the period are presented in the figure as well. The highest occurrence of organic aerosol concentration appeared nearly at 20 to 35 $\mu g\,m^{-3}$, corresponding with signal fraction of m/z 44 less than 2. The signal of m/z 44 showed an increasing trend with increasing organic mass. The lower concentration of organic

ACPD
14, 23375–23413, 2014

component mainly existed at RH below 40 %, which was indicative of a relatively clean atmosphere in urban Beijing. It was notable that the higher levels of the organic component occurred under high RH conditions, in which aerosol water uptake ability was enhanced and the more highly hydrated particles were able to capture more water-soluble volatile organic compounds (VOCs). In this way, the dry mass concentration of organic aerosol increased after the water evaporated in the AMS. The studies of Ge et al. (2012) in central valley of California and Dall'Osto et al. (2009) in London also showed that aqueous-phase processes were responsible for the production of secondary organic aerosol species, most significantly during fog events.

3.6 Sources apportionment of light scattering coefficient

3.6.1 A primarily determination of low RH aerosol light scattering hygroscopic growth factor *f*(RH)

During the measurement period, the atmosphere was stable with low wind speed ($2.5\,m\,s^{-1}$). We calculated the aerosol scattering hygroscopic growth factor with elevated relative humidity and fitted the scattering growth curve as shown in Fig. 11. The RH was divided into eight bins, and the average scattering coefficient in each RH bin was calculated. Here, the scattering coefficient at low RH conditions (RH < 40 %), with the average values of $549\,M\,m^{-1}$, was used as a normalizing factor 1, and scattering growth factors at higher RH values were calculated as: $f(\mathrm{RH} = 80\,\%) = \sigma_{sp}(\mathrm{RH} = 80\,\%)/\sigma_{sp}(\mathrm{RH} < 40\,\%)$. Then, an empirical equation containing two parameters can be used to fit the scattering factors at other RH bins as flowing;

$$f(\mathrm{RH}) = 1 + a(\mathrm{RH}/100)^b \quad (5)$$

As shown in Fig. 11, the fitting resulted in values of a and b of 2.9 and 3.0, respectively. At RH = 80 % the aerosol exhibited a strong scattering growth factor during this heavy pollution episode, with an *f*(RH) value of 2.41. The result is similar to reports by Pan et al. (2009) and Liu et al. (2008), in which they determined values of 2.33 to 2.48 at

ACPD
14, 23375–23413, 2014

RH = 90 % during a heavy pollution episode in urban Beijing and 2.04 to 2.68 at RH = 85 % in urban Guangzhou. Also, research by Kim et al. (2006) reported pollutants from east region of China had a f(RH) of 2.0 to 2.43 during local urban pollution episode in Gosan regional site.

3.6.2 Light scattering apportionment

Light scattering by atmospheric aerosols is highly dependent on their size, morphology and compositions (Liou, 2002). Sulfate, nitrate, ammonium and organic components in aerosol contribute most to light scattering, and particularly for diameters ranging from 100 nm to 1000 nm, they have the greatest light extinction efficiency (Seinfeld and Pandis, 1998). Here, a modified IMPROVE algorithm was employed to apportion light scattering coefficients at $\lambda = 550$ nm (Pitchford et al., 2007). The IMPROVE algorithm was based on a multiple liner regression method (Chan et al., 1999), which considers the degree to which aerosol light scattering is related to the mass concentration of each component combined with water uptake of inorganic component. The detailed introduction of the method can be can be found in Lowenthal et al. (1995).

In our light apportionment calculation, the mass concentrations of ammonium sulfate, ammonium nitrate, ammonium chloride and organic were required. However, the AMS can only provide us mass concentrations of sulfate, nitrate, ammonium chloride and organic compounds. Here, a commonly accepted ion pairing scheme of calculating the neutral aerosol from the molar number of all ions simplified by Gysel et al. (2007) is applied. In this scheme, by setting the fraction of nitric acid to zero, the molar fraction of ammonium nitrate is equal to the molar fraction of nitrate ions. The rest of ammonium ions are assigned to ammonium sulfate and ammonium chloride according to ammonium molar fraction. In our measurement period, ammonium is sufficient to neutralize those anions at most of the time, and the mass contribution from ammonium bisulfate can be ignored.

In our IMPROVE algorithm, the light scattering growth due to inorganic components were considered, while the contribution from organic aerosol was not as other studies.

ACPD
14, 23375–23413, 2014

Then, using the highly resolution mass concentrations of ammonium sulfate, ammonium nitrate, ammonium chloride and organic in submicron aerosol and fitted aerosol scattering growth curve in Sect. 3.6.1, we get a relationship of scattering coefficient and aerosol components and light scattering growth factor as showed in Eq. (6). The fitting was finished under MATLAB software (MATLAB R2010a). Figure 12a shows the time series of apportioned light scattering coefficients of each aerosol components compared with measured values during observation period. At the beginning of the periods, organic component dominated light scattering. With the development of the haze, the contribution of inorganic components increased as shown in Fig. 12b. The predicted values match the measured values, with a R^2 of 0.91 as showed in Fig. 13 and the correlation was better for the relatively cleaner time periods than that in more polluted times. The total average light scattering contribution of each aerosol component is presented in Fig. 14. The apportionment contributions from organic, ammonium sulfate, ammonium nitrate and ammonium chloride were 57.4 %, 22.5 %, 10.1 % and 10 %, respectively, which indicated the dominant contribution of organic and sulfate compounds to light scattering during this haze episode in Beijing. One should note that the apportioned light scattering coefficient using IMPROVE method is highly related with its mass concentration, and organic aerosol has a large mass fractions in it. A research by Yao et al. (2010) during winter in Shenzhen, PRC, using AMS data also showed high contribution (45 %) of light extinction due to organic components. A report by Watson (2002) also found the organic aerosol dominated light extinction in some cities, with fractions of 9–50 % in east USA.

$$\sigma_{sp}^{550} = (5.9 \pm 1.1) f(\mathrm{RH})[(NH_4)_2SO_4] + (1.1 \pm 0.4) f(\mathrm{RH})[NH_4NO_3] + (5.4 \pm 2.6) f(\mathrm{RH})[NH_4Cl] + (7.3 \pm 0.8)[\mathrm{organic}] + (74.4 \pm 26.7) \quad (6)$$

ACPD
14, 23375–23413, 2014

4 Summary and conclusion

Based on in-situ measurements, physical and chemical properties of aerosol particles were characterized during a severe haze episode during winter of 2013 in Beijing from 24 January through 31 January. The average mass concentrations of PM_1, $PM_{2.5}$ and PM_{10} were $99.1 \pm 67.1\ \mu g\,m^{-3}$, $188.3 \pm 128.8\ \mu g\,m^{-3}$ and $265.2 \pm 157.1\ \mu g\,m^{-3}$, and an increasing fraction of $PM_{1-2.5}$ was significant during the most heavy pollution periods. The averaged scattering coefficient ($\lambda = 550$ nm) was $877.2 \pm 624.2\ M\,m^{-1}$, and an increasing amount of relative coarse particle also can be seen from the variations of backscattering ratios, asymmetry parameter and scattering Ångström exponent. Particle number size distribution (14 nm to 2500 nm) showed high number concentrations in the nucleation and accumulation modes. Size-resolved chemical composition of submicron aerosol from a HR-ToF-AMS showed that the mass concentration of organic, sulfate, nitrate, ammonium and chlorine mainly resided on 500–800 nm in vacuum diameter, and sulfate and ammonium contributed to particle growth during the most heavily polluted day on 28 January.

High background pollutant emissions combined with stable synoptic conditions and increasing of relative humidity, which lead to enhanced water uptake ability of submicron aerosol and formation of secondary aerosol, may be the main reasons for the heavy haze episode. Light scattering apportionment showed that organic, ammonium sulfate, ammonium nitrate and ammonium chloride contributed to light scattering fractions of 57.4 %, 22.5 %, 10.1 % and 10 %, respectively. Considering their dominant fractional contribution to light scattering and light extinction, our study indicated that organic components also play an important role in visibility degradation in the winter haze episode in Beijing.

The Supplement related to this article is available online at doi:10.5194/acpd-14-23375-2014-supplement.

ACPD
14, 23375–23413, 2014

Acknowledgements. We acknowledge Professor Zhang Wu of Lanzhou University for help in nephelometer maintaining. This work was supported by National Natural Science Foundation of China (41230642), the CAS Strategic Priority Research Program grant XDA05100100 and XDB05020402.

References

Anderson, T. L., Charlson, R. J., Schwartz, S. E., Knutti, R., Boucher, O., Rodhe, H., and Heintzenberg, J.: Atmospheric science. Climate forcing by aerosol – a hazy picture, Science, 300, 1103–1104, doi:10.1126/science.1084777, 2003.

Andrews, E., Sheridan, P. J., Fiebig, M., McComiskey, A., Ogren, J. A., Arnott, P., Covert, D., Elleman, R., Gasparini, R., Collins, D., Jonsson, H., Schmid, B., and Wang, J.: Comparison of methods for deriving aerosol asymmetry parameter, J. Geophys. Res., 111, D05S04, doi:10.1029/2004JD005734, 2006.

Beddows, D. C. S., Dall'osto, M., and Harrison, R. M.: An enhanced procedure for the merging of atmospheric particle size distribution data measured using electrical mobility and time-of-flight analysers, Aerosol Sci. Technol., 44, 930–938, doi:10.1080/02786826.2010.502159, 2010.

Chan, Y. C., Simpson, R. W., McTainsh, G. H., Vowles, P. D., Cohen, D. D., and Bailey, G. M.: Source apportionment of visibility degradation problems in Brisbane (Australia) using the multiple linear regression techniques, Atmos. Environ., 33, 3237–3250, doi:10.1016/S1352-2310(99)00091-6, 1999.

Chen, J., Zhao, C. S., Ma, N., Liu, P. F., Göbel, T., Hallbauer, E., Deng, Z. Z., Ran, L., Xu, W. Y., Liang, Z., Liu, H. J., Yan, P., Zhou, X. J., and Wiedensohler, A.: A parameterization of low visibilities for hazy days in the North China Plain, Atmos. Chem. Phys., 12, 4935–4950, doi:10.5194/acp-12-4935-2012, 2012.

Cheng, Y. F., Su, H., Rose, D., Gunthe, S. S., Berghof, M., Wehner, B., Achtert, P., Nowak, A., Takegawa, N., Kondo, Y., Shiraiwa, M., Gong, Y. G., Shao, M., Hu, M., Zhu, T., Zhang, Y. H., Carmichael, G. R., Wiedensohler, A., Andreae, M. O., and Pöschl, U.: Size-resolved measurement of the mixing state of soot in the megacity Beijing, China: diurnal cycle, aging and parameterization, Atmos. Chem. Phys., 12, 4477–4491, doi:10.5194/acp-12-4477-2012, 2012.

ACPD
14, 23375–23413, 2014

Dall'Osto, M., Harrison, R. M., Coe, H., and Williams, P.: Real-time secondary aerosol formation during a fog event in London, Atmos. Chem. Phys., 9, 2459–2469, doi:10.5194/acp-9-2459-2009, 2009.
Deng, Z. Z., Zhao, C. S., Ma, N., Ran, L., Zhou, G. Q., Lu, D. R., and Zhou, X. J.: An examination of parameterizations for the CCN number concentration based on in situ measurements of aerosol activation properties in the North China Plain, Atmos. Chem. Phys., 13, 6227–6237, doi:10.5194/acp-13-6227-2013, 2013.
Garland, R. M., Yang, H., Schmid, O., Rose, D., Nowak, A., Achtert, P., Wiedensohler, A., Takegawa, N., Kita, K., Miyazaki, Y., Kondo, Y., Hu, M., Shao, M., Zeng, L. M., Zhang, Y. H., Andreae, M. O., and Pöschl, U.: Aerosol optical properties in a rural environment near the mega-city Guangzhou, China: implications for regional air pollution, radiative forcing and remote sensing, Atmos. Chem. Phys., 8, 5161–5186, doi:10.5194/acp-8-5161-2008, 2008.
Ge, X., Zhang, Q., Sun, Y., Ruehl, C. R., and Setyan, A.: Effect of aqueous-phase processing on aerosol chemistry and size distributions in Fresno, California, during wintertime, Environ. Chem., 9, 221, doi:10.1071/en11168, 2012.
Gysel, M., Crosier, J., Topping, D. O., Whitehead, J. D., Bower, K. N., Cubison, M. J., Williams, P. I., Flynn, M. J., McFiggans, G. B., and Coe, H.: Closure study between chemical composition and hygroscopic growth of aerosol particles during TORCH2, Atmos. Chem. Phys., 7, 6131–6144, doi:10.5194/acp-7-6131-2007, 2007.
He, H., Wang, Y., Ma, Q., Ma, J., Chu, B., Ji, D., Tang, G., Liu, C., Zhang, H., and Hao, J.: Mineral dust and NO_x promote the conversion of SO_2 to sulfate in heavy pollution days, Sci. Rep., 4, 4172, doi:10.1038/srep04172, 2014.
He, X., Li, C. C., Lau, A. K. H., Deng, Z. Z., Mao, J. T., Wang, M. H., and Liu, X. Y.: An intensive study of aerosol optical properties in Beijing urban area, Atmos. Chem. Phys., 9, 8903–8915, doi:10.5194/acp-9-8903-2009, 2009.
Hu, M., He, L., Huang, X., and Wu, Z.: Chemical and Physical Properties, Source and Formation of Fine and Ultrafine Particle in Beijing, Science Press, 2009.
Huang, K., Zhuang, G., Lin, Y., Li, J., Sun, Y., Zhang, W., and Fu, J. S.: Relation between optical and chemical properties of dust aerosol over Beijing, China, J. Geophys. Res., 115, D00K16, doi:10.1029/2009JD013212, 2010a.
Huang, X.-F., He, L.-Y., Hu, M., Canagaratna, M. R., Sun, Y., Zhang, Q., Zhu, T., Xue, L., Zeng, L.-W., Liu, X.-G., Zhang, Y.-H., Jayne, J. T., Ng, N. L., and Worsnop, D. R.: Highly time-resolved chemical characterization of atmospheric submicron particles during 2008 Beijing

ACPD
14, 23375–23413, 2014

Olympic Games using an Aerodyne High-Resolution Aerosol Mass Spectrometer, Atmos. Chem. Phys., 10, 8933–8945, doi:10.5194/acp-10-8933-2010, 2010b.
Kaufman, Y. J., Koren, I., Remer, L. A., Rosenfeld, D., and Rudich, Y.: The effect of smoke, dust, and pollution aerosol on shallow cloud development over the Atlantic Ocean, Proc. Natl. Acad. Sci. USA, 102, 11207–11212, doi:10.1073/pnas.0505191102, 2005.
Kim, J., Yoon, S.-C., Jefferson, A., and Kim, S.-W.: Aerosol hygroscopic properties during Asian dust, pollution, and biomass burning episodes at Gosan, Korea in April 2001, Atmos. Environ., 40, 1550–1560, doi:10.1016/j.atmosenv.2005.10.044, 2006.
Koren, I., Kaufman, Y. J., Rosenfeld, D., Remer, L. A., and Rudich, Y.: Aerosol invigoration and restructuring of Atlantic convective clouds, Geophys. Res. Lett., 32, L14828, doi:10.1029/2005GL023187, 2005.
Li, W. J., Shao, L. Y., and Buseck, P. R.: Haze types in Beijing and the influence of agricultural biomass burning, Atmos. Chem. Phys., 10, 8119–8130, doi:10.5194/acp-10-8119-2010, 2010.
Liu, X., Cheng, Y., Zhang, Y., Jung, J., Sugimoto, N., Chang, S.-Y., Kim, Y. J., Fan, S., and Zeng, L.: Influences of relative humidity and particle chemical composition on aerosol scattering properties during the 2006 Prd Campaign, Atmos. Environ., 42, 1525–1536, doi:10.1016/j.atmosenv.2007.10.077, 2008.
Liu, X. G., Li, J., Qu, Y., Han, T., Hou, L., Gu, J., Chen, C., Yang, Y., Liu, X., Yang, T., Zhang, Y., Tian, H., and Hu, M.: Formation and evolution mechanism of regional haze: a case study in the megacity Beijing, China, Atmos. Chem. Phys., 13, 4501–4514, doi:10.5194/acp-13-4501-2013, 2013.
Liu, Z. R., Hu, B., Liu, Q., Sun, Y., and Wang, Y. S.: Source apportionment of urban fine particle number concentration during summertime in Beijing, Atmos. Environ., 359–369, doi:10.1016/j.atmosenv.2014.06.055, 2014.
Liou, K. N.: An Introduction to Atmospheric Radiation, 2nd Edn., Elsevier Science, Elsevier Press, 2002.
Lohmann, U. and Feichter, J.: Global indirect aerosol effects: a review, Atmos. Chem. Phys., 5, 715–737, doi:10.5194/acp-5-715-2005, 2005.
Lowenthal, D. H., Rogers, C. F., Saxena, P., Watson, J. G., and Chow, J. C.: Sensitivity of estimated light extinction coefficients to model assumptions and measurement errors, Atmos. Environ., 29, 751–766, doi:10.1016/1352-2310(94)00340-Q, 1995.

ACPD
14, 23375–23413, 2014

Ma, N., Zhao, C. S., Müller, T., Cheng, Y. F., Liu, P. F., Deng, Z. Z., Xu, W. Y., Ran, L., Nekat, B., van Pinxteren, D., Gnauk, T., Müller, K., Herrmann, H., Yan, P., Zhou, X. J., and Wiedensohler, A.: A new method to determine the mixing state of light absorbing carbonaceous using the measured aerosol optical properties and number size distributions, Atmos. Chem. Phys., 12, 2381–2397, doi:10.5194/acp-12-2381-2012, 2012.

Meier, J., Wehner, B., Massling, A., Birmili, W., Nowak, A., Gnauk, T., Brüggemann, E., Herrmann, H., Min, H., and Wiedensohler, A.: Hygroscopic growth of urban aerosol particles in Beijing (China) during wintertime: a comparison of three experimental methods, Atmos. Chem. Phys., 9, 6865–6880, doi:10.5194/acp-9-6865-2009, 2009.

Nel, A.: Atmosphere. Air pollution-related illness: effects of particles, Science, 308, 804–806, doi:10.1126/science.1108752, 2005.

Pan, X. L., Yan, P., Tang, J., Ma, J. Z., Wang, Z. F., Gbaguidi, A., and Sun, Y. L.: Observational study of influence of aerosol hygroscopic growth on scattering coefficient over rural area near Beijing mega-city, Atmos. Chem. Phys., 9, 7519–7530, doi:10.5194/acp-9-7519-2009, 2009.

Pitchford, M., Malm, W., Schichtel, B., Kumar, N., Lowenthal, D., and Hand, J.: Revised algorithm for estimating light extinction from improve particle speciation data, J. Air Waste Manage. Assoc., 57, 1326–1336, doi:10.3155/1047-3289.57.11.1326, 2007.

Poschl, U.: Atmospheric aerosols: composition, transformation, climate and health effects, Angew. Chem. Int. Ed. Engl., 44, 7520–7540, doi:10.1002/anie.200501122, 2005.

Qu, W. J., Arimoto, R., Zhang, X. Y., Zhao, C. H., Wang, Y. Q., Sheng, L. F., and Fu, G.: Spatial distribution and interannual variation of surface PM_{10} concentrations over eighty-six Chinese cities, Atmos. Chem. Phys., 10, 5641–5662, doi:10.5194/acp-10-5641-2010, 2010.

Quan, J., Zhang, Q., He, H., Liu, J., Huang, M., and Jin, H.: Analysis of the formation of fog and haze in North China Plain (NCP), Atmos. Chem. Phys., 11, 8205–8214, doi:10.5194/acp-11-8205-2011, 2011.

Ramanathan, V., Crutzen, P. J., Kiehl, J. T., and Rosenfeld, D.: Aerosols, climate, and the hydrological cycle, Science, 294, 2119–2124, doi:10.1126/science.1064034, 2001.

Sakurai, H., Fink, M. A., McMurry, P. H., Mauldin, L., Moore, K. F., Smith, J. N., and Eisele, F. L.: Hygroscopicity and volatility of 4–10 Nm particles during summertime atmospheric nucleation events in urban Atlanta, J. Geophys. Res.-Atmos., 110, D22S04, doi:10.1029/2005JD005918, 2005.

Seinfeld, J. H. and Pandis, S. N.: Atmospheric Chemistry and Physics, from Air Pollution to Climate Changes, Wiley, New York, USA, 1998.

ACPD
14, 23375–23413, 2014

Shi, J. P., Evans, D. E., Khan, A. A., and Harrison, R. M.: Sources and concentration of nanoparticles (< 10 nm diameter) in the urban atmosphere, Atmos. Environ., 35, 1193–1202, doi:10.1016/S1352-2310(00)00418-0, 2001.

Sun, Y. L., Zhuang, G. S., Tang, A., Wang, Y., and An, Z.: Chemical characteristics of $PM_{2.5}$ and PM_{10} in haze-fog episodes in Beijing, Environ. Sci. Technol., 40, 3148–3155, doi:10.1021/es051533g, 2006.

Tang, G., Wang, Y., Li, X., Ji, D., Hsu, S., and Gao, X.: Spatial-temporal variations in surface ozone in Northern China as observed during 2009–2010 and possible implications for future air quality control strategies, Atmos. Chem. Phys., 12, 2757–2776, doi:10.5194/acp-12-2757-2012, 2012.

Titos, G., Foyo-Moreno, I., Lyamani, H., Querol, X., Alastuey, A., and Alados-Arboledas, L.: Optical properties and chemical composition of aerosol particles at an urban location: an estimation of the aerosol mass scattering and absorption efficiencies, J. Geophys. Res.-Atmos., 117, D04206, doi:10.1029/2011JD016671, 2012.

Twomey, S.: The Influence of pollution on the shortwave albedo of clouds, J. Atmos. Sci., 34, 1149–1152, 1977.

Wang, K. C., Dickinson, R. E., Su, L., and Trenberth, K. E.: Contrasting trends of mass and optical properties of aerosols over the Northern Hemisphere from 1992 to 2011, Atmos. Chem. Phys., 12, 9387–9398, doi:10.5194/acp-12-9387-2012, 2012.

Wang, L., Xu, J., Yang, J., Zhao, X., Wei, W., Cheng, D., Pan, X., and Su, J.: Understanding haze pollution over the Southern Hebei Area of China using the CMAQ model, Atmos. Environ., 56, 69–79, doi:10.1016/j.atmosenv.2012.04.013, 2012b.

Wang, Y., Yao, L., Wang, L., Liu, Z., Ji, D., Tang, G., Zhang, J., Sun, Y., Hu, B., and Xin, J.: Mechanism for the formation of the January 2013 heavy haze pollution episode over Central and Eastern China, Sci. China Earth Sci., 57, 14–25, doi:10.1007/s11430-013-4773-4, 2014a.

Wang, Y. H., Hu, B., Ji, D. S., Liu, Z. R., Tang, G. Q., Xin, J. Y., Zhang, H. X., Song, T., Wang, L. L., Gao, W. K., Wang, X. K., and Wang, Y. S.: Ozone weekend effects in the Beijing–Tianjin–Hebei metropolitan area, China, Atmos. Chem. Phys., 14, 2419–2429, doi:10.5194/acp-14-2419-2014, 2014b.

Watson, J. G.: Visibility: science and regulation, J. Air Waste Manage., 52, 628–713, doi:10.1080/10473289.2002.10470813, 2002.

ACPD
14, 23375–23413, 2014

Wehner, B., Birmili, W., Ditas, F., Wu, Z., Hu, M., Liu, X., Mao, J., Sugimoto, N., and Wiedensohler, A.: Relationships between submicrometer particulate air pollution and air mass history in Beijing, China, 2004–2006, Atmos. Chem. Phys., 8, 6155–6168, doi:10.5194/acp-8-6155-2008, 2008.

Willeke, K. and Baron. P. A.: Aerosol Measurement Principles, Techniques, and Applications, Van Nostrand Reinhold, Hoboken, NJ, 1993.

Wu, Z., Hu, M., Liu, S., Wehner, B., Bauer, S., Maßling, A., Wiedensohler, A., Petäjä, T., Dal Maso, M., and Kulmala, M.: New particle formation in Beijing, China: statistical analysis of a 1-year data set, J. Geophys. Res., 112, D09209, doi:10.1029/2006jd007406, 2007.

Yang, M., Howell, S. G., Zhuang, J., and Huebert, B. J.: Attribution of aerosol light absorption to black carbon, brown carbon, and dust in China – interpretations of atmospheric measurements during EAST-AIRE, Atmos. Chem. Phys., 9, 2035–2050, doi:10.5194/acp-9-2035-2009, 2009.

Yao, T., Huang, X., He, L., Hu, M., Sun, T., Xue, L., Lin, Y., Zeng, L., and Zhang, Y.: High time resolution observation and statistical analysis of atmospheric light extinction properties and the chemical speciation of fine particulates, Sci. China Chem., 53, 1801–1808, doi:10.1007/s11426-010-4006-z, 2010.

Zhang, J. K., Sun, Y., Liu, Z. R., Ji, D. S., Hu, B., Liu, Q., and Wang, Y. S.: Characterization of submicron aerosols during a month of serious pollution in Beijing, 2013, Atmos. Chem. Phys., 14, 2887–2903, doi:10.5194/acp-14-2887-2014, 2014.

Zhang, Q., Quan, J., Tie, X., Huang, M., and Ma, X.: Impact of aerosol particles on cloud formation: aircraft measurements in China, Atmos. Environ., 45, 665–672, doi:10.1016/j.atmosenv.2010.10.025, 2011.

Zhang, Q., Stanier, C. O., Canagaratna, M. R., Jayne, J. T., Worsnop, D. R., Pandis, S. N., and Jimenez, J. L.: Insights into the chemistry of new particle formation and growth events in Pittsburgh based on aerosol mass spectrometry, Environ. Sci. Technol., 38, 4797–4809, doi:10.1021/es035417u, 2004.

Zhang, Q. H., Zhang, J. P., and Xue, H. W.: The challenge of improving visibility in Beijing, Atmos. Chem. Phys., 10, 7821–7827, doi:10.5194/acp-10-7821-2010, 2010.

Zhang, X., Sun, J., Wang, Y., Li, W., Zhang, Q., Wang, W., Quan, J., Cao, G., Wang, J., Yang, Y., and Zhang, Y.: Factors contributing to haze and fog in China, Chin. Sci. Bull., 58, 1178, doi:10.1360/972013-150, 2013 (Chinese Version).

ACPD
14, 23375–23413, 2014

Zhang, X. Y., Wang, Y. Q., Niu, T., Zhang, X. C., Gong, S. L., Zhang, Y. M., and Sun, J. Y.: Atmospheric aerosol compositions in China: spatial/temporal variability, chemical signature, regional haze distribution and comparisons with global aerosols, Atmos. Chem. Phys., 12, 779–799, doi:10.5194/acp-12-779-2012, 2012.

Zhao, X. J., Zhao, P. S., Xu, J., Meng„ W., Pu, W. W., Dong, F., He, D., and Shi, Q. F.: Analysis of a winter regional haze event and its formation mechanism in the North China Plain, Atmos. Chem. Phys., 13, 5685–5696, doi:10.5194/acp-13-5685-2013, 2013.

ACPD
14, 23375–23413, 2014

Table 1. The statistic of aerosol optical properties during observation period.

Parameter	Mean	Median	Standard derivation	5 % quantile	95 % quantile
σ_{sp}^{450} (M m^{-1})	1088.5	924.4	748.1	48.1	2386.3
σ_{sp}^{550} (M m^{-1})	877.2	748.4	624.2	36.6	1993.4
σ_{sp}^{700} (M m^{-1})	718.4	628.2	530.9	28.7	1703.3
σ_{bsp}^{450} (M m^{-1})	134.4	122.8	87.1	7.6	281.4
σ_{bsp}^{550} (M m^{-1})	108.1	96.4	71	6.1	228.5
σ_{bsp}^{700} (M m^{-1})	98.7	89.3	66.5	7.3	214.4
b_{450}	0.13	0.13	0.02	0.11	0.16
b_{550}	0.14	0.12	0.02	0.11	0.17
b_{700}	0.15	0.14	0.02	0.13	0.19
$Å_{450/550}$	1.2	1.3	0.3	0.74	1.7
$Å_{550/700}$	0.94	1.0	0.3	0.41	1.4
g_{450}	0.58	0.6	0.04	0.52	0.62
g_{550}	0.57	0.6	0.05	0.50	0.63
g_{700}	0.54	0.56	0.05	0.46	0.60

ACPD
14, 23375–23413, 2014

Table 2. The statistic of particle number concentration during observation period.

Parameter	Mean	Median	Standard derivation	5 % quantile	95 % quantile
Nucleation (cm^{-3})	1.90×10^5	1.8×10^5	8.3×10^4	6.3×10^4	3.4×10^5
Aitken (cm^{-3})	1.5×10^6	1.4×10^6	6.4×10^5	5.7×10^5	2.7×10^6
Accumulation (cm^{-3})	1×10^6	9.9×10^6	3.9×10^5	4.7×10^5	1.6×10^6
Coarse (cm^{-3})	3.1×10^3	2.9×10^3	2.3×10^3	2.5×10^2	7.0×10^3

ACPD
14, 23375–23413, 2014

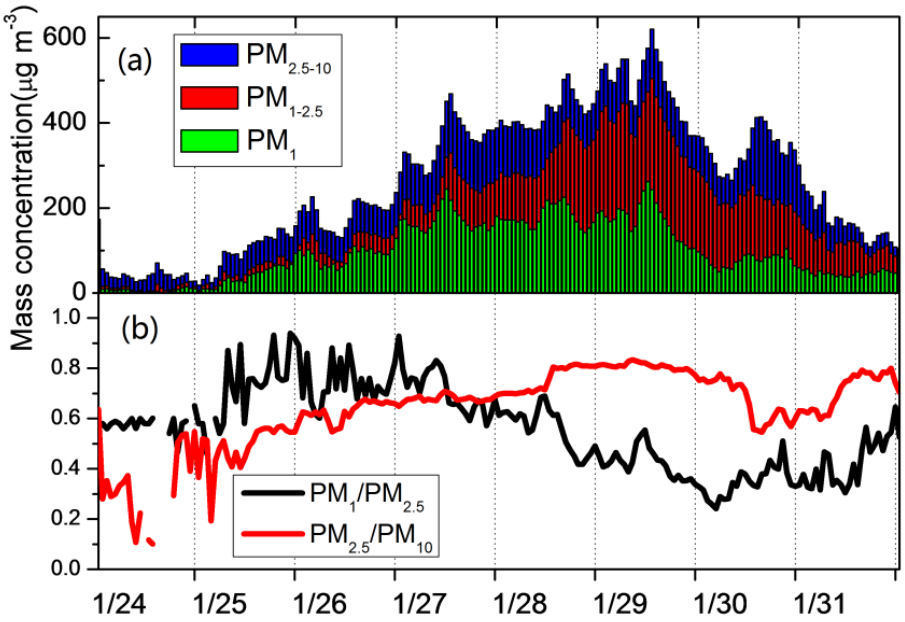

Figure 1. Time series of **(a)** mass concentrations of PM_1, $PM_{1-2.5}$ and $PM_{2.5-10}$, **(b)** mass ratios of $PM_1/PM_{2.5}$ and $PM_{2.5}/PM_{10}$.

ACPD
14, 23375–23413, 2014

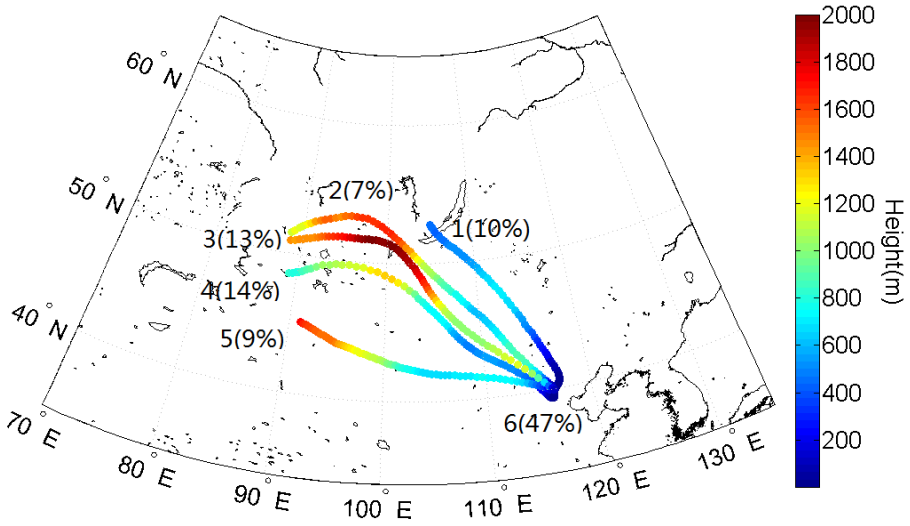

Figure 2. The three days backward trajectory of air parcels during the observation period; the colors of air trajectories represent height during transport.

ACPD
14, 23375–23413, 2014

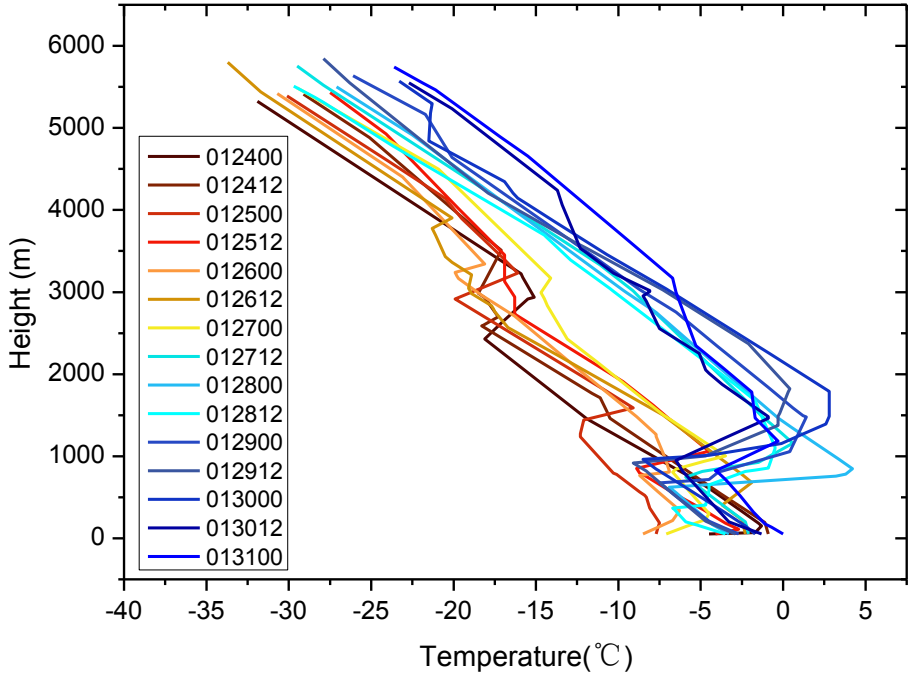

Figure 3. The temperature profiles during observation period. The legend stands for UTC time. For example, 012400 means 0:00 on 24 January.

ACPD
14, 23375–23413, 2014

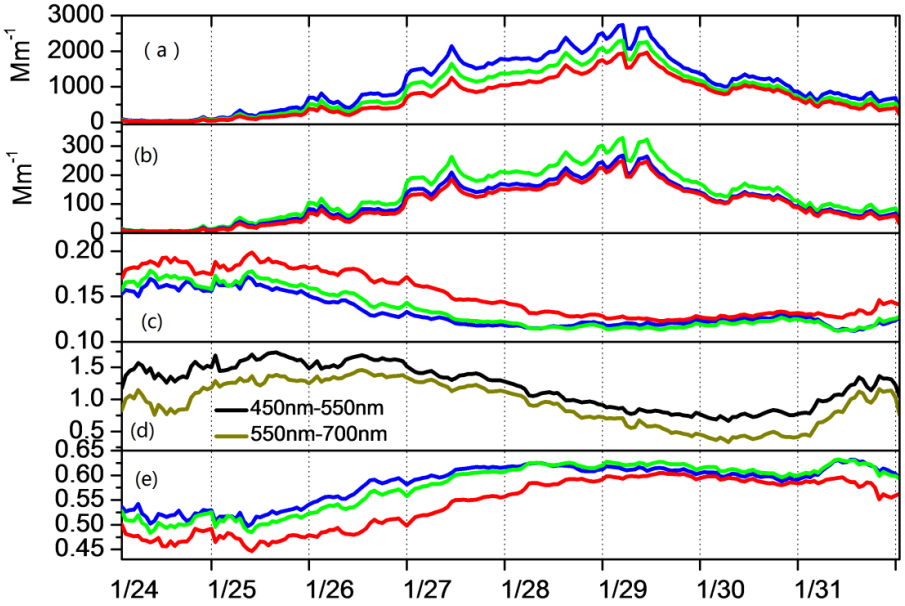

Figure 4. Time series of **(a)** scattering coefficients σ_{sp}, **(b)** backscattering coefficients σ_{bsp}, **(c)** backscattering ratios b_λ, **(e)** asymmetry parameter g_λ at wavelengths of 450 nm (blue), 550 nm (green) and 700 nm (red) **(d)** scattering Ångström exponent ($Å_{sp}$) from 450–550 nm (black) and 550–700 nm(brown).

ACPD
14, 23375–23413, 2014

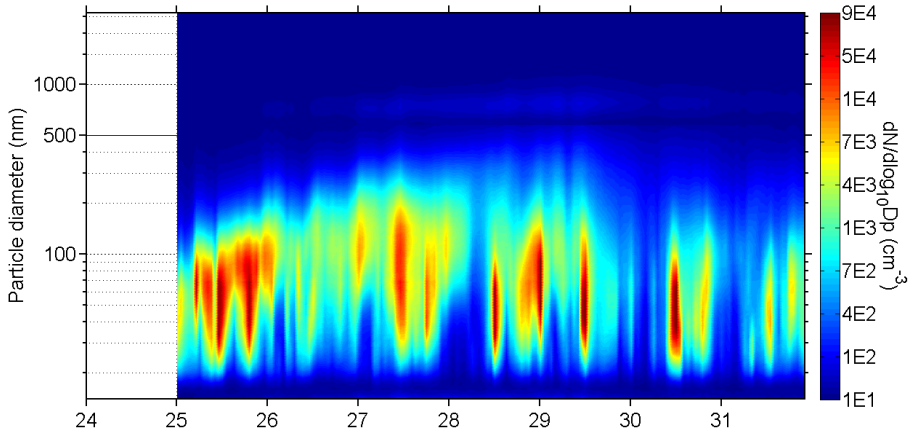

Figure 5. Particle number size distribution between 14.1–2458 nm using SMPS combined with APS from 25 to 31 January. The *x* axis represents the data of January and *y* axis represents particle diameter (nm). The color in the Fig. 5 represents particle concentration ($dN/d\log D_p$).

ACPD
14, 23375–23413, 2014

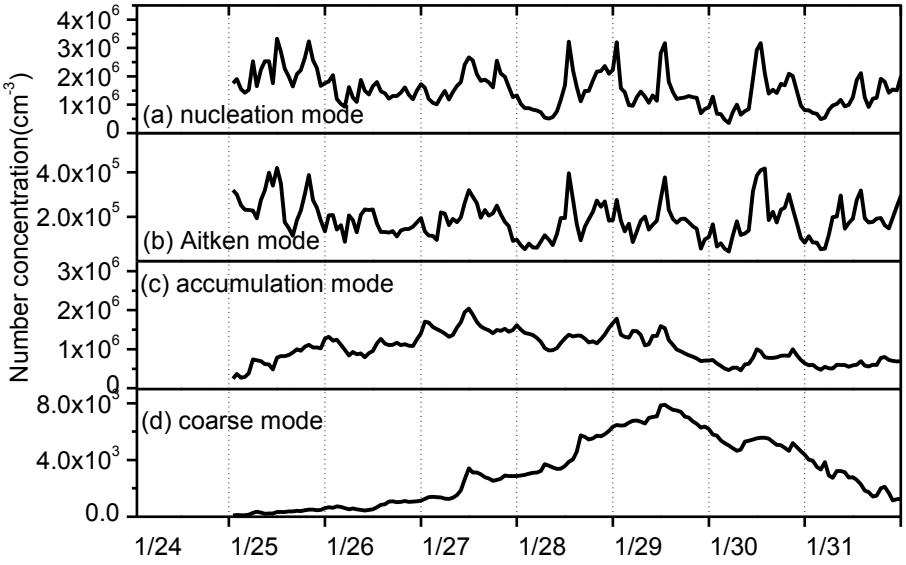

Figure 6. Number concentrations of **(a)** nucleation mode (14.1–25 nm), **(b)** Aitken mode (25–100 nm), **(c)** accumulation mode (100–1000 nm) and **(d)** coarse mode (1000–2458 nm) from 25 January to 31 January.

ACPD
14, 23375–23413, 2014

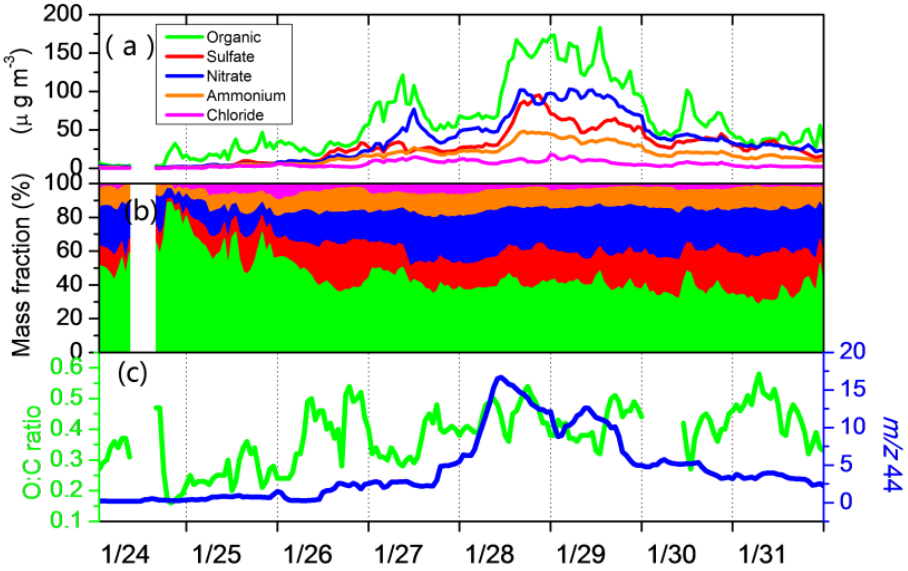

Figure 7. Time series of **(a)** mass concentrations of organic, sulfate, nitrate, ammonium and chloride in submicron aerosol **(b)** mass fractions of organic, sulfate, nitrate, and ammonium and chloride **(c)** O : C ratio and m/z 44 during the haze episode.

ACPD
14, 23375–23413, 2014

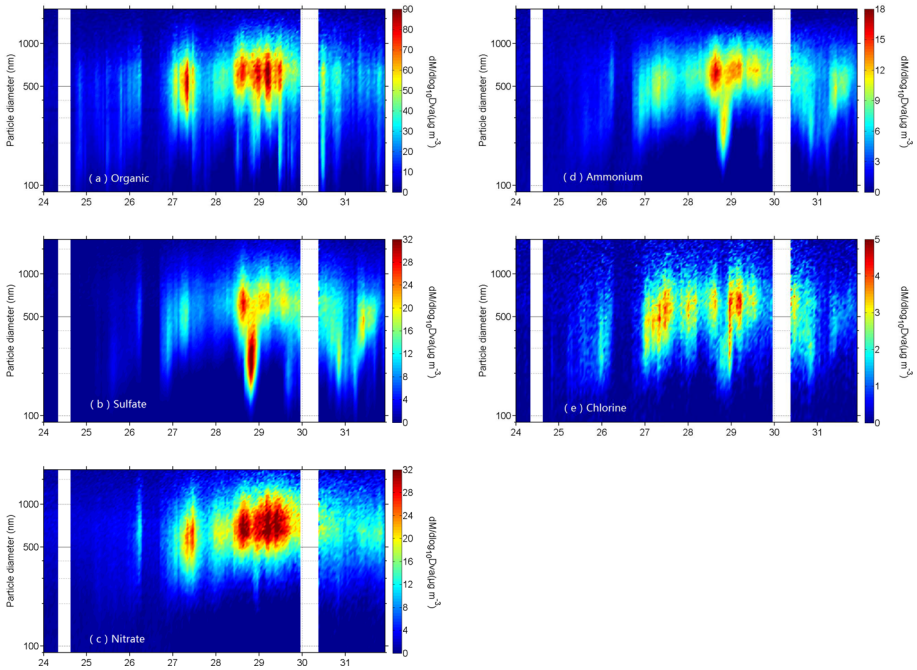

Figure 8. Size-resolved chemical compositions of **(a)** organic **(b)** sulfate **(c)** nitrate **(d)** ammonium and **(e)** chlorine.

ACPD
14, 23375–23413, 2014

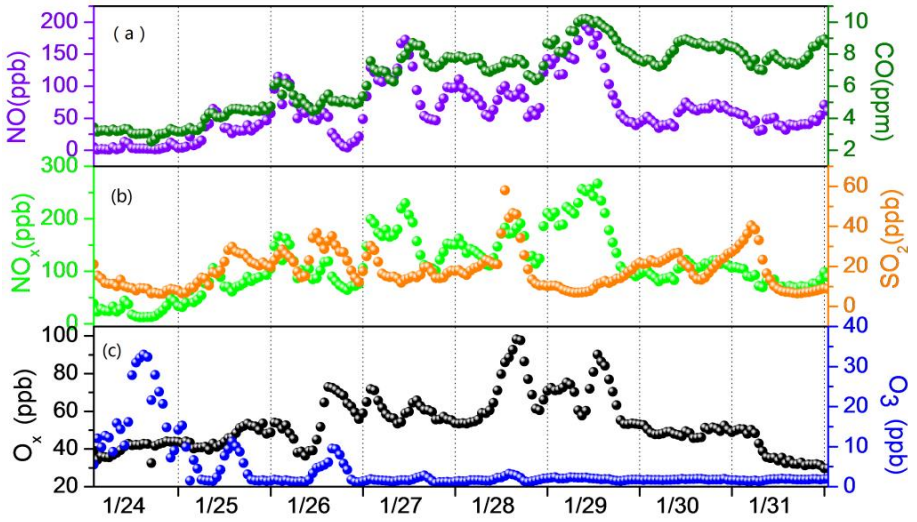

Figure 9. Mixing ratios of **(a)** NO and CO **(b)** NO_x and SO_2 **(c)** O_x and O_3.

ACPD
14, 23375–23413, 2014

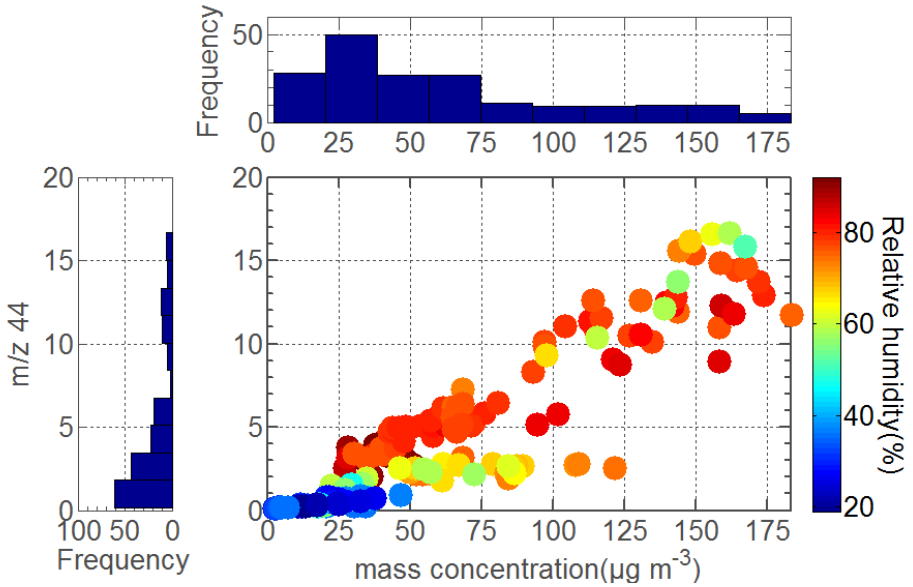

Figure 10. (Left panel) The frequency distribution of m/z 44, (top panel) the frequency distribution of organic mass, (center panel) abundance of m/z 44 as a function of organic aerosol mass concentration and the influence of RH (left, color scale).

ACPD
14, 23375–23413, 2014

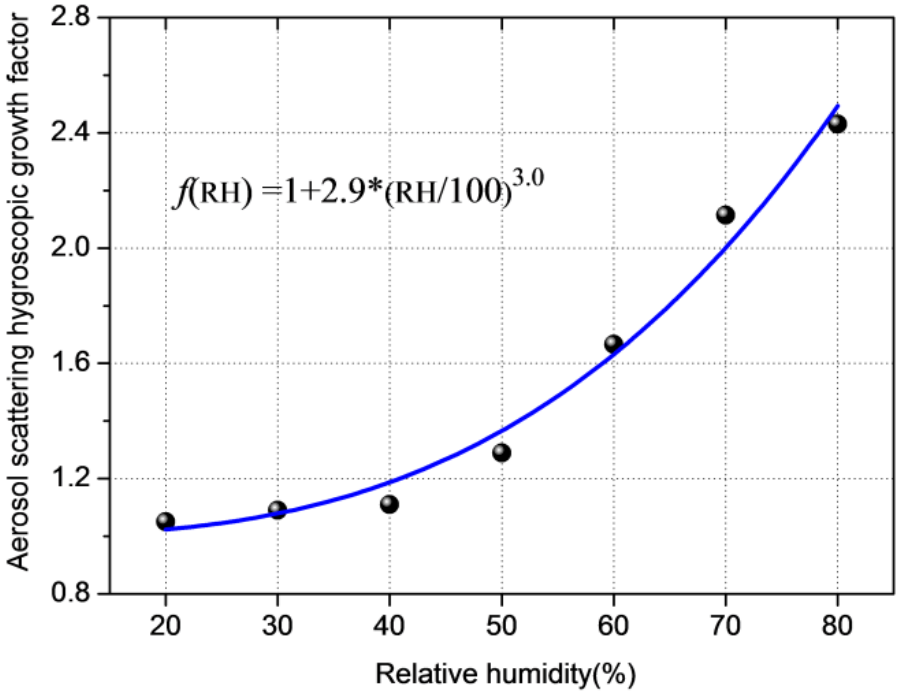

Figure 11. The fitting curve of aerosol light scattering growth factor. The data points represent the measured scattering coefficient averaged over different RH bins.

ACPD
14, 23375–23413, 2014

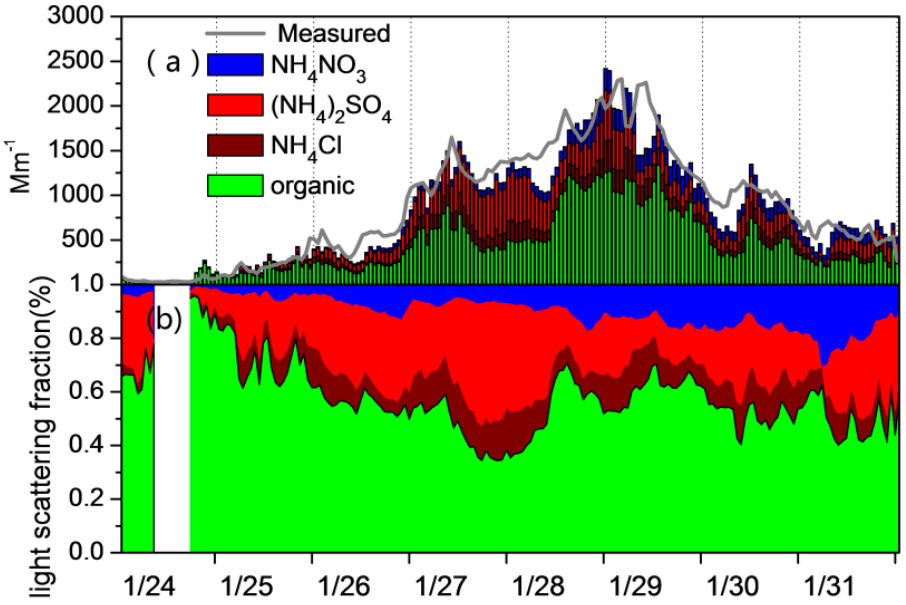

Figure 12. Time series of **(a)** apportioned light scattering coefficients of each aerosol components compared with measured **(b)** light scattering fractions of each aerosol components.

ACPD
14, 23375–23413, 2014

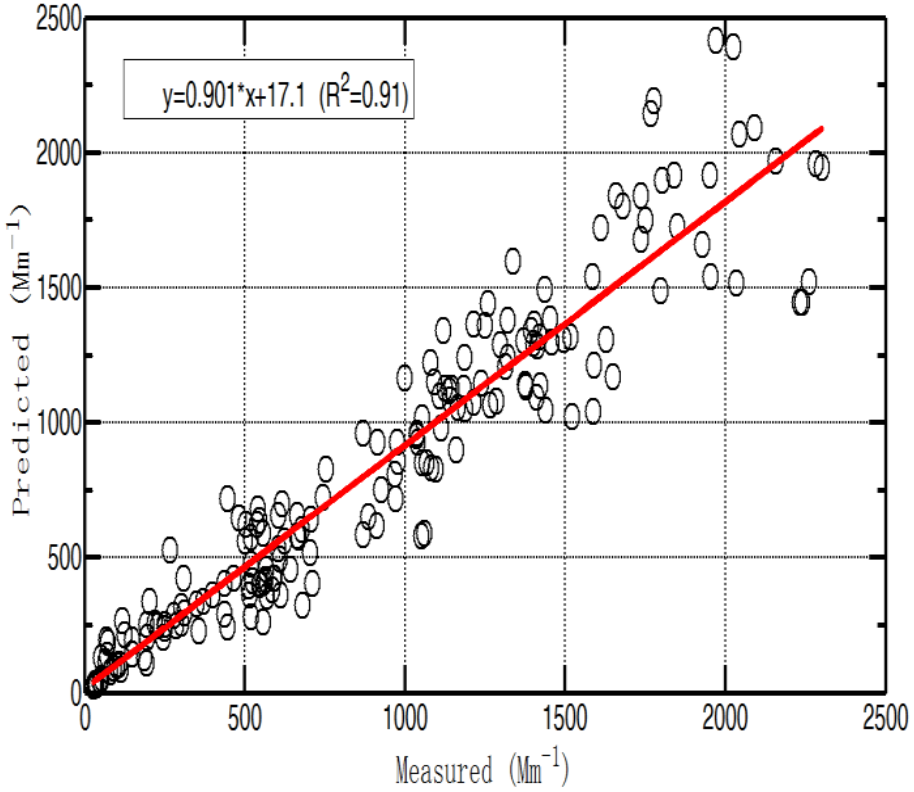

Figure 13. Correlation between measured light scattering coefficient at 550 nm and predicted using IMPROVE method.

ACPD
14, 23375–23413, 2014

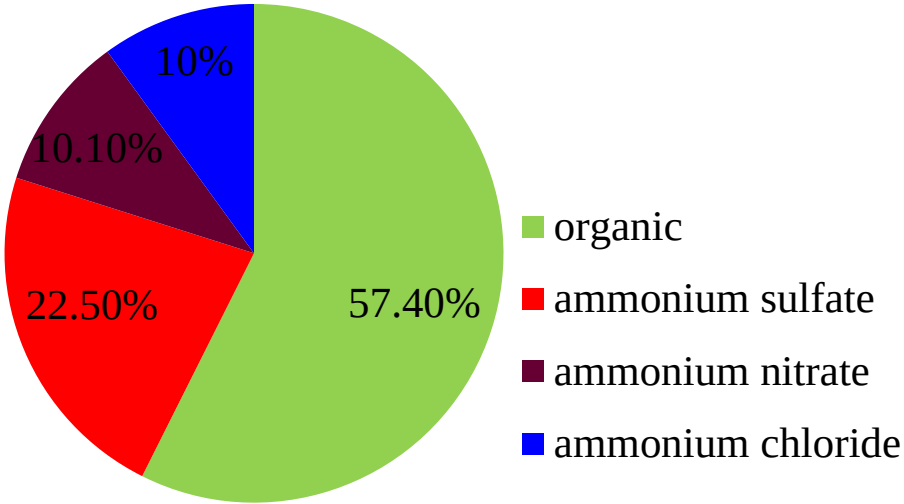

Figure 14. Averaged light scattering contribution of each aerosol components during the haze episode.

ACPD
14, 23375–23413, 2014